The Canadian Mineralogist
Vol. 58, pp. 637-652 (2020)
DOI: 10.3749/canmin.2000044

CRYSTAL STRUCTURE DETERMINATION OF KOSNARITE, $KZr_2(PO_4)_3$, FROM THE MARIO PINTO MINE, JENIPAPO DISTRICT, ITINGA, BRAZIL

PAULA C. PIILONEN[§]

Beaty Centre for Species Discovery, Research and Collections Division, Canadian Museum of Nature, P.O. Box 3443, Station D, Ottawa, Ontario K1P 6P4, Canada

HENRIK FRIIS

Natural History Museum, University of Oslo, Postboks 1172, Blindern, 0318 Oslo, Norway

RALPH ROWE AND GLENN POIRIER

Beaty Centre for Species Diversity, Research and Collections Division, Canadian Museum of Nature, P.O. Box 3443, Station D, Ottawa, Ontario K1P 6P4, Canada

ABSTRACT

The crystal structure of a natural kosnarite, $KZr_2(PO_4)_3$ from the Mario Pinto Mine, Jenipapo district, Brazil, has been determined for the first time. Kosnarite and its related synthetic compounds (NZP) are open-framework orthophosphates of the type $(^{[6]}M'^{[8]}M'')L_2(TO_4)_3$ (where M = Li, Na, K, Rb, Cs; L = Ti, Zr, Hf; and T = P, Si). These compounds have been proposed as potential radioactive waste hosts as a result of their physiochemical properties and because their crystal structure allows for extreme isomorphism and incorporation of all 42 radioactive nuclides present in nuclear waste. Kosnarite from the Mario Pinto mine is hexagonal, $R\bar{3}c$, with $a = 8.7205(1)$, $c = 23.9436(3)$ Å, and $V = 1576.89(4)$ Å^3. The average chemical formula ($n = 75$) is $(K_{0.96}Na_{0.02})_{\Sigma 0.98}(Zr_{1.93}Hf_{0.08})_{\Sigma 1.01}(P_{2.99}Si_{0.01})_{\Sigma 3.00}O_{12}$. The structure contains one six-coordinated Zr site (L), one four-coordinated P site (T), and a six-coordinated K site (M'); in kosnarite, the M'' site is vacant. The average bond lengths in the ZrO_6 octahedra (2.0646 Å) and PO_4 tetrahedra (1.5278 Å) are slightly larger than those observed in the synthetic analogue (<Zr–O> = 2.063 Å, <P–O> = 1.522 Å). The ZrO_6 octahedra and PO_4 tetrahedra share corners to form ribbons of $[Zr_2(PO_4)_3]^-$ units parallel to the **c** axis, which are further joined by PO_4 tetrahedra perpendicular to **c** to form a 3D network. Kosnarite is one of only five natural alkali zircono-orthophosphates, all of which are late-stage hydrothermal minerals. Although synthetic Na-dominant endmember analogues of kosnarite exist, the distortions in the structure with respect to the M and L octahedra, along with experimental evidence at hydrothermal temperatures, suggest that only K (or Li) endmembers are possible in nature.

Keywords: kosnarite, crystal structure, zircono-orthophosphates, hydrothermal, granitic pegmatite.

INTRODUCTION

Kosnarite, $KZr_2(PO_4)_3$, was first described from the Mount Mica and Black Mountain granitic pegmatites in Oxford county, Maine (Brownfield *et al*. 1993), where it occurs as a late-stage secondary mineral in association with other phosphates including eosphorite, fluorapatite, moraesite, and triphylite. It has since been described from granitic pegmatites in other localities, including Wycheproof, Victoria, Australia (Birch *et al*. 1994); the Limoeiro mine, Virgem de Lapa, Brazil (Hyrsl *et al*. 2003); the Chaquicocha gold deposit, Yanacocha district, Peru (Deditius *et al*. 2015); and the Mario Pinto and Jorge pegmatites, Taquaral pegmatite field, Jenipapo area, Brazil (Frost *et al*. 2012, Menezes Filho *et al*. 2016).

Kosnarite from the type locality is scarce and, as such, no structure determination was made when the

[§] *Corresponding author e-mail address*: ppiilonen@nature.ca

mineral was described. However, synthetic compounds isostructural to kosnarite have been extensively studied since the 1960s. The crystal structure of sodium zirconium phosphate [NZP, $NaZr_2(PO_4)_3$; space group $R\bar{3}c$, $Z = 6$)] was first determined in 1968 (Hagman & Kierkegaard 1968) and that of the isostructural synthetic $KZr_2(PO_4)_3$ material was determined the following year (Šljukić *et al*. 1969). Kosnarite and its related synthetic compounds are open-framework orthophosphates of the type $([^{[6]}M'^{[8]}M'')L_2(TO_4)_3$ (where M = Li, Na, K, Rb, Cs; L = Ti, Zr, Hf; and T = P, Si). The physiochemical properties of these insoluble, single-phase crystalline ceramics are ideal for the immobilization of high-level radioactive waste and radionuclides. Synthetic NZP materials are environmentally safe, have high chemical and thermal stability, show extremely low thermal expansion, and are insoluble under aqueous conditions and leach-resistant. Sodium zirconium phosphate was first proposed as a potential radioactive waste host (Roy *et al*. 1983) for its physiochemical properties and because its crystal structure allows for extreme isomorphism and incorporation of almost two-thirds of the periodic table, including all 42 radioactive nuclides present in nuclear waste. Extensive studies have been done on more than 150 possible NZP compounds to determine the effects of various substitutions on the crystal structure in order to develop ceramic structures that can be tailored and tuned to the waste products to be removed and immobilized.

Occurrence

The Mario Pinto Mine (coordinates: –16.672443 –41.869686) is located in the Taquaral pegmatite field (Jenipapo, Itinga county), which is one of the subdivisions of the Eastern Brazilian Pegmatite (EBP) province (Frost *et al*. 2012, Menezes Filho *et al*. 2016). The pegmatite is medium-grained, composed dominantly of muscovite and feldspar with an irregular quartz core having a maximum thickness of 15 m. Kosnarite is a secondary hydrothermal mineral that occurs in miarolitic cavities as beige to pale yellow druses of euhedral, pseudocubic crystals up to 3 mm associated with albite and sprays of zanazziite (Fig. 1). The kosnarite sample in this study (CMNMC 87568) was obtained from Brian R. Kosnar, the son of Richard A. Kosnar for whom the mineral was named.

Fig. 1. Yellowish-beige psueodocubic kosnarite from the Mario Pinto Mine, Jenipapo, Brazil (3 × 5 cm). Photo by M. Bainbridge.

Chemical Composition

Chemical analyses of kosnarite were obtained with a JEOL Superprobe 8230 operating in the wavelength-dispersive mode and using Probe for EMPA Extreme Edition software (https://www.probesoftware.com/) at the University of Ottawa. Operating conditions were as follows: beam diameter of 10 μm, operating voltage 20 kV, and a beam current of 50 nA. A total of 21 elements were sought and the following standards and X-ray lines were employed: sanidine (K $K\alpha$, Si $K\alpha$, Al $K\alpha$), albite (Na $K\alpha$), synthetic diopside (Mg $K\alpha$, Ca $K\alpha$), rutile (Ti $K\alpha$), columbite-(Mn) (Nb $L\alpha$, Mn $K\alpha$), zircon (Zr $L\alpha$), hematite (Fe $K\alpha$), celestine (Sr $L\alpha$), pollucite (Cs $L\alpha$), sanbornite (Ba $L\alpha$), Rb-microcline (Rb $L\alpha$), gahnite (Zn $K\alpha$), topaz (F $K\alpha$), synthetic UO_2 (U $M\alpha$), synthetic ThO_2 (Th $M\alpha$), synthetic hafnon (Hf $M\alpha$), and fluorapatite (P $K\alpha$). Count times for all elements were 20 s on peak and 20 s on background. Raw intensities were converted to concentrations using the default φρZ corrections of the Probe for EMPA software package (Armstrong 1988). Elemental interferences were corrected using empirical overlap corrections. Table 1 contains the EMPA data and formula calculation normalized to 12 anions, as well as average data from previous studies of kosnarite.

Powder X-Ray Diffraction

Powder X-ray diffraction (pXRD) data were collected using a Bruker D8 discover-MR A25 instrument equipped with a Dectris Eiger2 R 500K detector. The instrument uses an Incoatec Cu micro-

TABLE 1. ELECTRON MICROPROBE COMPOSITIONS OF KOSNARITE

	This study Grain 1 ($n = 7$)		This study Grain 2 ($n = 28$)		This study Grain 3 ($n = 40$)		Brownfield *et al.* 1993		Birch *et al.* 1994	Menezes Filho *et al.* 2016 ($n = 5$)		Deditius *et al.* 2015 ($n = 10$)	
Element	Avg.	Range	Avg.	Range	Avg.	Range	Mt. Mica ($n = 8$)	Black Mtn. ($n = 11$)	($n = 6$)	Avg.	Range	Ave	Range
K_2O (wt.%)	8.83	8.58–8.98	8.82	7.86–9.02	8.83	8.59–9.02	8.70	9.25	8.46	9.236	9.04–9.51	8.76	8.28–9.14
Na_2O	0.13	0.01–0.38	0.12	0.03–1.09	0.13	0.01–0.77	1.40	bdl	0.04			0.10	0.0–0.18
Rb_2O	0.00	0.00	0.00	0.00	0.00	0.00	0.25	0.20	0.11			0.63	0.11–1.05
Cs_2O	0.00	0.00–0.01	0.02	0.00–0.52	0.01	0.00–0.17			0.03				
CaO	0.00	0.00–0.01	0.02	0.00–0.54	0.00	0.00–0.02							
FeO	0.01	0.00–0.04	0.01	0.00–0.06	0.01	0.00–0.14	0.20	bdl	0.15	0.022	0.00–0.08	0.10	0.06–0.13
MnO	0.01	0.00–0.04	0.01	0.00–0.16	0.01	0.00–0.12	1.00	bdl	0.54				
MgO	0.01	0.00–0.05	0.00	0.00–0.04	0.01	0.00–0.04				0.024	0.00–0.06		
SrO	0.02	0.00–0.05	0.03	0.00–0.09	0.03	0.00–0.08			0.3				
BaO	0.02	0.00–0.04	0.02	0.00–0.04	0.01	0.00–0.05			0.09				
Al_2O_3	0.00	0.00–0.02	0.00	0.00	0.00	0.00–0.02			0.28	0.014	0.00–0.04	0.04	0.02–0.06
SiO_2	0.06	0.00–0.26	0.03	0.00–0.08	0.06	0.00–0.39			0.34	0.026	0.00–0.05	0.09	0.03–0.19
TiO_2	0.00	0.00–0.01	0.00	0.00–0.02	0.01	0.00–0.02						0.07	0.05–0.09
ZrO_2	46.52	45.17–47.61	46.49	43.98–48.99	46.60	45.25–48.75	44.50	47.90	46.1	46.494	45.64–47.51	45.49	42.79–48.00
HfO_2	3.21	1.79–4.53	3.29	0.87–4.84	3.26	0.88–5.05	0.50	0.90	1.79	2.354	2.08–2.97	4.10	0.31–7.61
P_2O_5	41.83	41.31–42.49	41.73	41.07–42.64	41.56	40.82–42.34	43.30	42.20	42.11	41.62	40.52–42.28	41.46	40.02–42.33
Nb_2O_5	0.05	0.00–0.15	0.04	0.00–0.10	0.05	0.00–0.11							
F	0.00	0.00–0.00	0.00	0.00	0.00	0.00	0.20	0.20	0.09				
O=F	0.00	0.00	0.00	0.00	0.00	0.00	0.08	0.08	0.04				
Total	100.73	99.94–101.12	100.65	99.38–101.63	100.60	99.48–101.64	99.97	100.57	100.56	99.78	99.21–100.10	100.59	99.52–101.53
apfu M site													
K^+	0.95	0.92–0.97	0.95	0.86–0.97	0.96	0.94–0.97	0.93	0.99	0.90	1.00	0.98–1.04	0.95	0.92–0.99
Na^+	0.02	0.00–0.06	0.02	0.01–0.18	0.02	0.00–0.13	0.08	0.00	0.01			0.03	0.01–0.05
Rb^+	0.00	0.00	0.00	0.00	0.00	0.00	0.01	0.01	0.01			0.03	0.01–0.06
Ca^{2+}	0.00	0.00	0.00	0.00–0.05	0.00	0.00							
Sr^{2+}	0.00	0.00	0.00	0.00	0.00	0.00			0.01				
Cs^{2+}	0.00	0.00	0.00	0.00–0.02	0.00	0.00–0.01							
Ba^{2+}	0.00	0.00	0.00	0.00	0.00	0.00							

TABLE 1. CONTINUED.

	This study Grain 1 ($n = 7$)		This study Grain 2 ($n = 28$)		This study Grain 3 ($n = 40$)		Brownfield *et al.* 1993		Birch *et al.* 1994	Menezes Filho *et al.* 2016 ($n = 5$)		Deditius *et al.* 2015 ($n = 10$)	
Element	Avg.	Range	Avg.	Range	Avg.	Range	Mt. Mica ($n = 8$)	Black Mtn. ($n = 11$)	($n = 6$)	Avg.	Range	Ave	Range
apfu L site													
Zr^{4+}	1.92	1.89–1.95	1.92	1.84–2.00	1.93	1.87–1.99	1.81	1.96	1.88	1.93	1.88–1.99	1.89	1.81–1.98
Hf^{4+}	0.08	0.04–0.11	0.08	0.02–0.12	0.08	0.02–0.12	0.01	0.02	0.17	0.06	0.05–0.07	0.10	0.01–0.19
Nb^{5+}	0.00	0.00–0.01	0.00	0.00	0.00	0.00							
Ti^{4+}	0.00	0.00	0.00	0.00	0.00	0.00						0.00	0.00–0.01
Fe^{2+}	0.00	0.00	0.00	0.00	0.00	0.00–0.01	0.01	bdl	0.01			0.01	0.00–0.01
Mn^{2+}	0.00	0.00	0.00	0.00–0.01	0.00	0.00–0.01	0.07	bdl	0.04				
Mg^{2+}	0.00	0.00–0.01	0.00	0.00–0.01	0.00	0.00–0.01				0.00	0.00–0.01		
apfu T site													
P^{5+}	3.00	2.98–3.02	3.00	2.98–3.01	2.99	2.94–3.02	3.06	3.00	2.98	3.00	2.95–3.03	2.99	2.95–3.02
Si^{4+}	0.01	0.00–0.02	0.00	0.00–0.01	0.00	0.00–0.03			0.01	0.00	0.00	0.01	0.00–0.02
Al^{3+}	0.00	0.00	0.00	0.00	0.00	0.00			0.03	0.00	0.00	0.00	0.00–0.01
F^{-}	0.00	0.00	0.00	0.00	0.00	0.00	0.05	0.05	0.09				
Scations	5.98	5.97–5.99	5.98	6.00–6.08	5.99	5.96–6.07	6.03	6.18	6.14	6.00	5.98–6.04	6.00	5.97–6.00
Zr/Hf	28	17–45	30	16–95	30	15–94	181	98	11	34	26–39	52	10–283

Birch *et al.* (1994) also included 0.17 wt.% Li_2O (0.06 Li *apfu*).

focus source (IμS) operating at 50 kV and 1 mA. The sample was mounted on a 250 μm spherical powder pin. A statistical approach (Rowe 2009) was used to calibrate the image-correction parameters (sample-to-detector distance and X-Y beam center coordinates). Further data correction was achieved with a residual error correction curve obtained with an NBS Si 640a standard and tested with an annealed fluorite standard. The resulting 2θ correction curve was applied to an XY data file (with a 0.005° step size) of the diffractogram to fix the instrumentation error, which results in a 2θ error of below ±0.001° for the whole diffraction pattern for diffraction peaks and features.

The sample yielded sharp diffraction peaks up to the maximum range of the experiment (132° 2θ). A Rietveld refinement of the pXRD data was performed using Bruker DiffracPlus Topas Rietveld software (http://www.bruker-axs.de/xrd_software.html), which gave a unit cell of $a = 8.717609(13)$, $b = 23.94183(6)$ Å, and $V = 1576.734(6)$ Å^3. The powder X-ray diffraction data are reported in Table 2, with a comparison to the synthetic (Powder Diffraction File 35-756) and published Mount Mica data from Brownfield *et al*. (1993). Only measured peaks from 0 to 80° with relative intensities of 2% or more were reported, but many sharp diffraction peaks were observed below 0.5% intensities, which greatly influenced the quality of the Rietveld unit-cell refinement.

Single-Crystal X-Ray Diffraction

A crystal of kosnarite was selected for single-crystal X-ray diffraction studies on the basis of optical homogeneity. Structural data were collected with a Rigaku Synergy-S diffractometer equipped with a HyPix-6000HE detector housed at the Natural History Museum, University of Oslo, Norway. A PhotonJet-S microfocus sealed tube operating at 50 kV and 1 mA provided the monochromatized Mo$K\alpha$ radiation. Data were collected at room temperature with a fixed detector-to-crystal distance of 34 mm. A full sphere of data was collected with a total of 3150 frames (12,961 reflections), frame widths of 0.20° ω, and exposure times of 2.35 s. Rigaku's CrysAlis Pro software was used to process the intensity data ($R_{int} = 0.0179$) and perform a shape-based absorption correction. Table 3 contains all information relevant to the data collection and crystal-structure determination.

The Oscail interface (McArdle 2017) which implements the SHELX-97 package of programs (Sheldrick 1997) was used for the solution and refinement of the crystal structure. Phasing of a set of normalized structure factors gave a mean $|E^2 - 1| = 1.109$, consistent with a centrosymmetric space group (predicted values: 0.968 for centrosymmetric and 0.736 for non-centrosymmetric). The space-group $R\bar{3}c$ was selected based on the low calculated combined figure of merit. The structure was solved by Patterson methods and refined in space group $R\bar{3}c$ with scattering curves taken from Cromer & Mann (1968) and Cromer & Liberman (1970). An *E*-map was produced using calculated phase-normalized factors which allowed one Zr, one P, and two oxygen atoms to be located. The structure was further refined based on F^2 for all unique data. The remaining cation (K) position was located using difference-Fourier maps during the refinement process. Refinement of the site occupancy factors for the Zr and K sites suggested the presence of heavier and lighter scatterers, respectively. In accordance with the EMP data, Hf was refined along with Zr, and Na with K. Site scattering values from the single-crystal refinement match those from the average EMP data. Table 4 contains all atomic coordinates and displacement factors, and Table 5 contains bond-length information. Distortion parameters were calculated for kosnarite and its synthetic equivalents (Table 5) to determine the effects of substitutions on the framework. The normalized bond-length variation or distortion (Δ), of the polyhedron was calculated using the equation:

$$\Delta \equiv \left\{ \sum_{i=1}^{n} [(l_i - l_m) l_m]^2 / n \right\} \cdot 10^4 \qquad (1)$$

(Brown & Shannon 1973, Shannon 1976) where l_i = bond length, l_m = mean bond length, and n = coordination number. The tetrahedral- and octahedral-angle variance [TAV (σT) and OAV (σM and σL), respectively)], alternate measures of polyhedral distortion, can be calculated using the following equations (Robinson *et al*. 1971):

$$\mathrm{TAV} = \sigma T^2 = \sum_{i=1}^{6} [(\mathrm{O} - T - \mathrm{O}) - 109.47]^2 \Big/ 5 \qquad (2)$$

$$\mathrm{OAV} = \sigma L, M^2 = \sum_{i=1}^{12} [(\mathrm{O} - (M, L) - \mathrm{O}) - 90]^2 \Big/ 11 \qquad (3)$$

Chemical Composition

Kosnarite from the Mario Pinto mine approaches endmember $KZr_2(PO_4)_3$ in its chemical composition, as has also been observed in kosnarite from an another unknown pegmatite in the Jenipapo district (Frost *et al*. 2012). The average chemical formula (n = 75) is $(K_{0.96}Na_{0.02})_{\Sigma 0.98}(Zr_{1.93}Hf_{0.08})_{\Sigma 1.01}(P_{2.99}Si_{0.01})_{\Sigma 3.00}O_{12}$.

TABLE 2. COMPARATIVE POWDER X-RAY DIFFRACTION DATA FOR KOSNARITE

Jenipapo District, Brazil (this study)					Syn. PDF35-756		Mount Mica (Brownfield *et al.* 1993)			
I obs.	*d* obs.	*I* calc. *	*d* calc. **	*hkl*	*I* calc. *	*d calc.*	*I* obs.	*d* obs.	*d* calc. **	*hkl*
25	6.383	22	6.386	012	12	6.393	50	6.41	6.36	012
42	4.689	40	4.691	104	27	4.695	50	4.679	4.676	104
83	4.358	88	4.359	110	66	4.363	100	4.329	4.343	110
73	3.825	70	3.826	113	62	3.828	90	3.806	3.813	113
36	3.193	35	3.193	024	38	3.194	40	3.167	3.182	204
100	2.943	100	2.944	116	100	2.944	90	2.928	2.934	116
8	2.834	7	2.834	211	9	2.835	5	2.816	2.823	211
5	2.782	5	2.782	018	7	2.783				
9	2.576	7	2.576	214	9	2.576	5	2.561	2.567	214
33	2.517	33	2.517	300	34	2.517	50	2.502	2.507	300
4	2.345	4	2.345	208	6	2.345				
2	2.283	3	2.283	1.0.10	4	2.283	3	2.279	2.276	1.0.10
4	2.271	4	2.271	119	8	2.271	3	2.263	2.264	119
2	2.191	2	2.191	217	3	2.192				
5	2.179	6	2.180	220	6	2.180	10	2.169	2.172	220
16	2.129	14	2.129	036	17	2.129	10	2.120	2.122	306
		2	2.129	306						
2	2.102	2	2.103	223	3	2.103				
10	2.065	9	2.063	128	12	2.066	8	2.054	2.059	218
									2.056	312
8	2.022	7	2.022	0.2.10	9	2.022	8	2.013	2.016	2.0.10
3	1.9953	3	1.9952	0.0.12	4	1.9953				
8	1.9764	7	1.9765	134	9	1.9769	8	1.971	1.970	134
30	1.9128	33	1.9127	226	31	1.9129	45	1.903	1.906	226
3	1.8644	2	1.8644	042	4	1.8645				
20	1.8342	20	1.8342	2.1.10	20	1.8343	40	1.826	1.829	2.1.10
4	1.7859	4	1.7858	137	5	1.7860	5	1.784	1.780	137
6	1.7158	7	1.7157	318	6	1.7157	15	1.711	1.710	318
4	1.6680	4	1.6679	0.1.14	5	1.6681				
8	1.6638	7	1.6638	324	9	1.6640	15	1.660	1.658	324
20	1.6476	23	1.6475	410	20	1.6478	35	1.641	1.641	410
2	1.6137	2	1.6135	413	3	1.6137	3	1.605	1.607	2.2.10
3	1.5966	4	1.5965	048	4	1.5965				
13	1.5763	12	1.5763	1.3.10	11	1.5763	8	1.570	1.571	1.3.10
7	1.5635	3	1.5634	3.0.12	8	1.5637				
		4	1.5634	0.3.12						
7	1.5579	9	1.5577	2.0.14	10	1.5578	13	1.552	1.553	2.0.14
14	1.5229	9	1.5228	146	13	1.5230	25	1.518	1.518	416
		9	1.5228	416						
2	1.4990	1	1.4991	238						
		2	1.4988	1.1.15	2	1.4990				
4	1.4824	4	1.4822	4.0.10	4	1.4824	8	1.477	1.477	4.0.10
8	1.4672	4	1.4678	1.0.16	2	1.4673	5	1.464	1.463	1.0.16
		7	1.4668	1.2.14					1.463	1.2.14
		3	1.4641	054	10	1.4641				
5	1.4530	6	1.4529	330	6	1.4533	8	1.447	1.448	330
3	1.4035	3	1.4033	3.2.10	3	1.4035	3	1.400	1.399	3.2.10
2	1.3880	2	1.3879	244	2	1.3882	3	1.386	1.387	2.0.16
									1.386	335
3	1.3654	5	1.3652	336	3	1.3655	5	1.362	1.361	336
		3	1.3252	2.1.16						

TABLE 2. CONTINUED.

Jenipapo District, Brazil (this study)					Syn. PDF35-756		Mount Mica (Brownfield *et al.* 1993)			
I obs.	*d* obs.	*I* calc. *	*d* calc. **	*hkl*	*I* calc. *	*d calc.*	*I* obs.	*d* obs.	*d* calc. **	*hkl*
6	1.3247	6	1.3245	3.1.14	8	1.3248	35	1.320	1.320	3.1.14
6	1.3227	6	1.3224	514	9	1.3225			1.318	514
2	1.2607	2	1.2605	517	5	1.2605	25	1.256	1.256	517
4	1.2584	6	1.2583	060	3	1.2885				
2	1.2258	2	1.2256	2.4.10						
5	1.2172	5	1.2169	2.3.14			3	1.214	1.214	3.1.16
									1.213	3.2.14
3	1.2091	5	1.2089	520						

* Calculated from kosnarite structural CIF file (this study)

** Calculated from XRPD rietveld refined cell $a = 8.717609(13)$, $b = 23.94183(6)$ Å, $V = 1576.734(6)$ Å^3

TABLE 3. EXPERIMENTAL AND CRYSTAL STRUCTURE DATA FOR KOSNARITE

Crystal data	
Crystal system, space group	Trigonal, $R\bar{3}c$
a (Å)	8.7205(1)
c (Å)	23.9436(3)
V (Å^3)	1576.89(4)
Z	6
Crystal Shape	blocky
Crystal Size	0.037 × 0.054 × 0.122 mm
m (Mo$K\alpha$)	2.893
Calculated density (g/cm^3)	3.199
Data collection	
Instrument	Rigaku XtalLAB Synergy
Radiation, wavelength	Mo$K\alpha$, 0.71073
Operating conditions	Room temperature
θ range (°)	2.56–35.84
Absorption correction	Gaussian integration of a multifaceted crystal model, spherical harmonics
No. of observed, unique and observed [$F_o > 4\sigma(F_o)$] reflections	12961, 791, 775
Mean I/σ	29.61
R_{int}	0.179
$\|E^2 - 1\|$	1.109
Min/Max Indices	$-13 < h < 14$, $-14 < k < 13$, $-37 < l < 35$
Refinement	
No. of reflections	791
No. of *l.s.* parameters	31
Final R index for all data	0.0115
Final R index for observed data	0.0110
wR^2	0.0349
GooF	1.238
$\Delta\rho_{max}$, $\Delta\rho_{min}$ (e$^-$ Å^{-3})	0.37, –0.49
$R = \Sigma(\|F_o\| - \|F_c\|)/\Sigma\|F_o\|$	
$wR^2 = [\Sigma(w)F_o^2 - F_c^2)^2/\Sigma[w(F_o^2)^2]^{1/2}$, $w = 1/\sigma^2(F_o)$	

In back-scattered electron and cathodoluminescence images (BSEI and CL, respectively), kosnarite exhibits oscillatory compositional zoning, with $K^+ \leftrightarrow Na^+$ and $Zr^{4+} \leftrightarrow Hf^{4+}$ being the dominant substitution mechanisms; minor Si^{4+} (up to 0.03 *apfu*) substituting for P^{4+} was also detected. Grain 1 shows a Hf-enriched band towards the rim of the crystal, with the core Hf-depleted and enriched in Na (Fig. 2A, B, C). Grain 2 also shows

TABLE 4. ATOMIC COORDINATES AND ISOTROPIC DISPLACEMENT FACTORS (Å × 10^3)

Atom	x	y	z	U_{11}	U_{22}	U_{33}	U_{23}	U_{13}	U_{12}	U_{eq}
(K,Na)	1.00000	1.00000	0.50000	0.05288(43)	0.05288(43)	0.00887(31)	0.00000	0.00000	0.02644(22)	0.03821(32)
(Zr,Hf)	0.66667	0.33333	0.68366(2)	0.00515(6)	0.00515(6)	0.00428(7)	0.00000	0.00000	0.00258(3)	0.00486(5)
P	0.66667	0.62076(3)	0.58333	0.00681(12)	0.00582(10)	0.00631(12)	–0.00073(4)	–0.00146(8)	0.00340(6)	0.00620(8)
O1	0.82702(9)	0.80170(9)	0.59612(3)	0.01110(28)	0.00947(26)	0.01334(28)	–0.00459(20)	–0.00247(21)	0.00095(22)	0.01317(13)
O2	0.62291(10)	0.50061(10)	0.63435(3)	0.01926(32)	0.01615(31)	0.01365(28)	0.00744(24)	0.00059(24)	0.01069(26)	0.01553(14)

an Hf-enriched band at the rim, with Na-enrichment towards the core, however Hf-rich zones are more patchy and suggestive of sector zoning towards the bottom of the crystal (Fig. 2D, E, F). The grains contain up to 0.18 *apfu* Na, the highest value recorded in a natural kosnarite sample to date, and up to 0.12 *apfu* Hf, which is close to the highest values recorded in a sample from the Chaquicocha high-sulfidation gold deposit in Peru (Deditius *et al*. 2015). No other elements contribute significantly to the observed compositional zoning.

Crystal Structure

Kosnarite from Brazil is hexagonal, $R\bar{3}c$, with $a = 8.7205(1)$, $c = 23.9436(3)$ Å, and $V = 1576.89(4)$ Å^3. It is isostructural with synthetic $KZr(PO_4)_3$ and other NZP materials (Table 5). The general formula is $(^{[6]}M'^{[8]}M'')L_2(TO_4)_3$, where M = alkali, alkaline earth, rare-earth, and actinide elements with charges from +1 to +4, including Li, Na, K, Rb, Cs; L = Ti, Zr, Hf, U, Th; and T = P, Si. The structure contains one six-coordinated Zr site (L), one four-coordinated P site (T), and a six-coordinated K site (M'); in kosnarite, the M'' site is vacant. Average bond lengths in the ZrO_6 octahedra (2.0646 Å) and PO_4 tetrahedra (1.5278 Å) are slightly larger than those observed in the synthetic analogue (<Zr–O> = 2.063 Å, <P–O> = 1.522 Å). The ZrO_6 octahedra and PO_4 tetrahedra share corners to form ribbons of $[Zr_2(PO_4)_3]^-$ units parallel to the **c** axis, which are further joined by PO_4 tetrahedra perpendicular to **c** to form a 3D network (Fig. 3A). This results in the formation of two void spaces, M' and M'', which can be filled by monovalent and divalent alkali and alkaline earth cations (Fig. 3B). The M sites act as buffers when the framework is distorted by substitutions and also compensate for framework charge imbalances. In synthetic NZP, it is possible for both M sites to be partially occupied ($M'_{1-x}M''_x$), but in natural kosnarite, which displays a very narrow range of compositions and limited substitutions, the M' site is 100% occupied [$(K_{0.967}Na_{0.033})$, <M'–O> = 2.8203(7) Å] and M'' is vacant.

Although >150 synthetic compositions exist with the basic $[L_2(PO_4)_3]^{n-}$ framework, few major structural parameter changes can be observed amongst them (Orlova *et al*. 2002). The basic structure of any NZP is extremely flexible and can suffer a range of distortions without breaking framework bonds (Alamo & Roy 1986). This is accomplished through rotations of the ZrO_6 and PO_4 polyhedra in opposite directions in response to the size and valence of the M cations (Alamo & Roy 1986). For the same size L cation (*e.g.*, Zr), an increase in the size of M results in a contraction in the **a** direction and an expansion in the **c** direction

TABLE 5. SELECT BOND LENGTHS (Å) AND DISTORTION PARAMETERS FOR KOSNARITE AND RELATED SYNTHETICS

Atom	Kosnarite	[1]$KZr_2(PO4)_3$	[2]$NaZr_2(PO_4)_3$	[3]$(Na_{0.5}K_{0.5})Hf_2(PO_4)_3$	[4]$Na(NbZr)_2(PO_4)_3$	[5]$(Na_{0.9}Cs_{0.1})Zr_2(PO_4)_3$	[5]$(Na_{0.8}Cs_{0.2})Zr_2(PO_4)_3$	[5]$(Na_{0.6}Cs_{0.4})Zr_2(PO_4)_3$	[6]$LiZr_2(PO_4)_3$	[7]$CsZr_2(PO_4)_3$	[8]$KU_2(PO_4)_3$
Space group	$R\bar{3}c$	$R\bar{3}c$	$R\bar{3}c$	$R\bar{3}c$	$R\bar{3}c$	$R\bar{3}c$	$R\bar{3}c$	$R\bar{3}c$	$R\bar{3}c$	$R\bar{3}c$	$R\bar{3}c$
a (Å)	8.7205(1)	8.71(1)	8.8043(2)	8.7295(1)	8.776(2)	8.8623(10)	8.80841(1)	8.80997(1)	8.847(1)	8.5758(2)	9.113(1)
c (Å)	23.9436(3)	23.89(2)	22.7585(9)	23.2023(4)	22.430(10)	22.7551(4)	22.7544(5)	22.7540(5)	22.24(3)	24.9061(4)	24.997(1)
Z	6	6	6	6	6	6	6	6	6	6	6
[6]*L* where *L* = Zr, Hf, Ti, Nb, U, Np, Pu											
Zr, Hf *apfu*	Zr 1.93, Hf 0.07	Zr 2, Hf 0	Zr 2, Hf 0	Zr 0, Hf 2	Zr 1, Nb 1	Zr 2	Zr 2	Zr2	Zr 2	Zr 2	Zr 0, U 2
L–O(2) × 3	2.0553(6)	2.061(9)	2.048(13)	2.069(5)	2.00(3)	2.02863(2)	2.02999(3)	2.02687(0)	2.039(3)	1.998(16)	2.30(14)
L–O(1) × 3	2.0740(6)	2.065(9)	2.084(12)	2.072(5)	2.063(18)	2.07406(2)	2.06890(3)	2.07281(2)	2.082(3)	2.16(2)	2.27(2)
<*L*–O>					2.033	2.0513	2.0494	2.0498	2.0603	2.0803	2.2944
ΔL	1.0030	1.0029	1.0054	1.0035	1.0046	1.0026	1.0025	1.0027	1.0028	1.0124	1.0071
σL	10.5561	10.2946	19.0023	12.7919	15.5377	8.9411	8.7865	9.3573	9.7193	37.9516	24.5804
[6]*M* where *M* = K, Na, Cs, Rb, Li											
K, Na *apfu*	K 0.97, Na 0.03	K 1, Na 0	K 0, Na 1	K 0.5, Na 0.5	K 0, Na 1	Na 0.9, Cs 0.1	Na 0.8, Cs 0.2	Na 0.6, Cs 0.4	Li 1	Cs 1	K 1, Na 0
M–O(1) × 6	2.8203(7)	2.812(9)	2.538(12)	2.651(4)	2.55(2)	2.59187(3)	2.5883(4)	2.58849(4)	2.501(3)	2.89(2)	2.907(19)
ΔM	1.2585	1.2607	1.162	1.2051	1.1522	1.1675	1.1695	1.1694	1.1215	1.3094	1.2068
σM	976.947	984.3633	6305956	788.6281	593.8348	650.9429	658.463	657.9933	476.7616	1148.0493	794.9885
[4]P											
P–O(1) × 2	1.5272(7)	1.511(9)	1.516(13)	1.508(6)	1.52(3)	1.51960	1.51676(0)	1.51253(0)	1.526(2)	1.52(3)	1.502(14)
P–O(2) × 2	1.5282(7)	1.533(9)	1.546(13)	1.524(4)	1.537(14)	1.53528	1.54441(3)	1.54925(3)	1.519(2)	1.54(3)	1.52(2)
<P–O>	1.5278	1.5228	1.536	1.5161	1.527	1.5274	1.5306	1.5309	1.5225	1.5284	1.5109
ΔP	1.0005	1.0006	1.0005	1.0023	1.0025	1.0018	1.0016	1.0018	1.0002	1.003	1.0172
σP	1.7934	2.0840	1.8765	9.5919	9.117	6.8386	6.1532	7.0772	0.8531	10.5494	73.8562

[1] Šljukić *et al.* (1969); [2] Hagman & Kierkegaard (1968); [3] Asabina *et al.* (2010); [4] Bennouna *et al.* (1995); [5] Chourasia *et al.* (2010); [6] Petit *et al.* (1986); [7] Gobechiya *et al.* (2004); [8] Gobechiya *et al.* (2005).

Δ = quadratic elongation, σ = bond angle variance; Robinson *et al.* (1971).

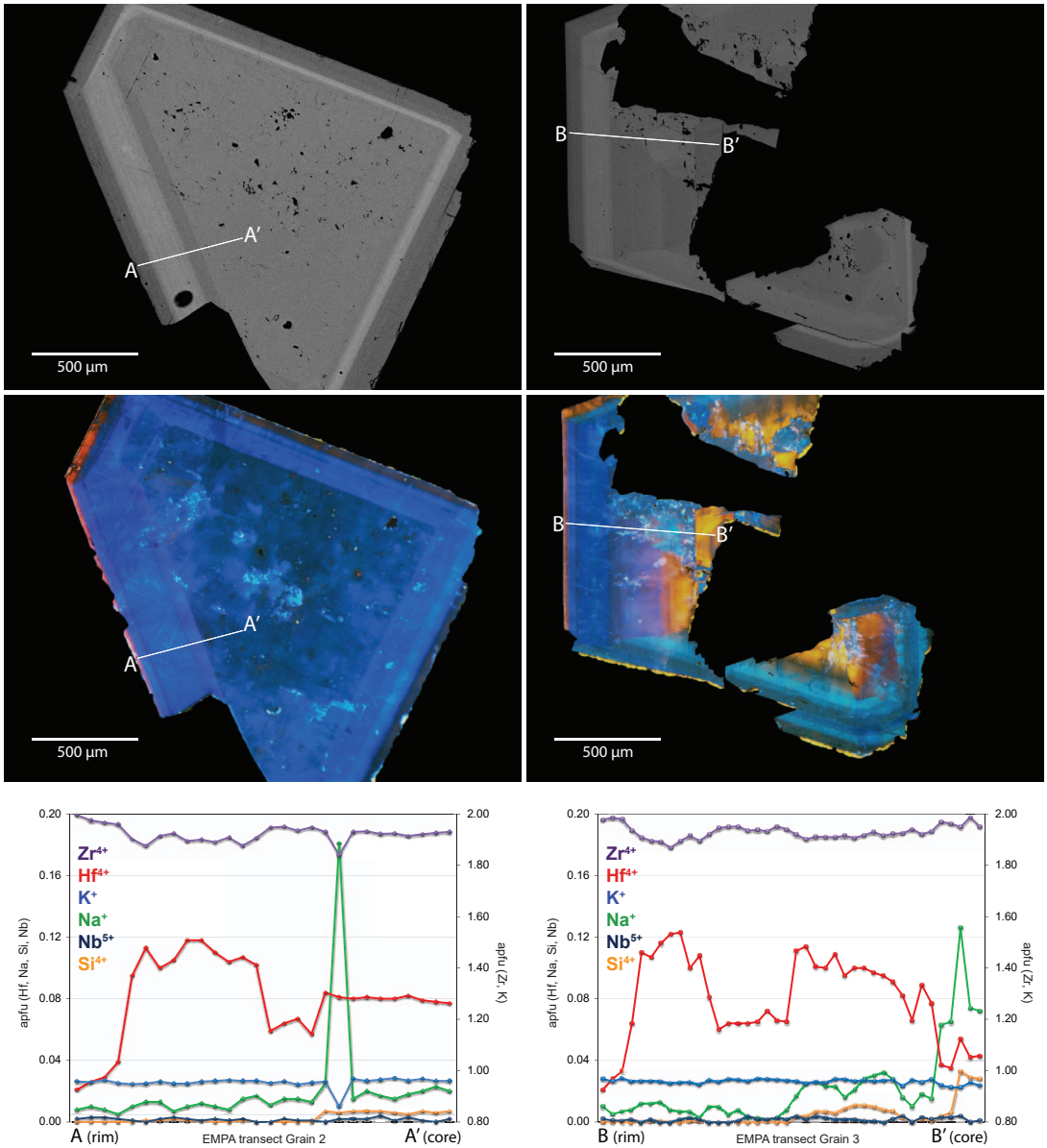

FIG. 2. Back-scattered (top) and cathodoluminescence (middle) images of kosnarite showing oscillatory zoning. Electron microprobe analyses from rim to core (bottom) show increasing Na, Hf, and Si in the cores of both crystals.

(Fig. 4). At the *L* site, an increase in the size of the cation results in an increase in both the *a* and *c* dimensions (Fig. 4) (Alamo & Roy 1986, Orlova 2002). In addition, distortion of the *M* site (σM) increases with increasing ionic radius of the *M*-site cation (Fig. 5A). The size of the cation at the *M* site also has an influence on the distortion of the *L* site, although it is not as pronounced (Fig. 5B). The Cs endmember composition results in the highest σL, yet those compositions with a mixed Cs-Na *M* site and an average ionic radius closest to the pure K endmember display lower σL, similar to what is observed in natural kosnarite.

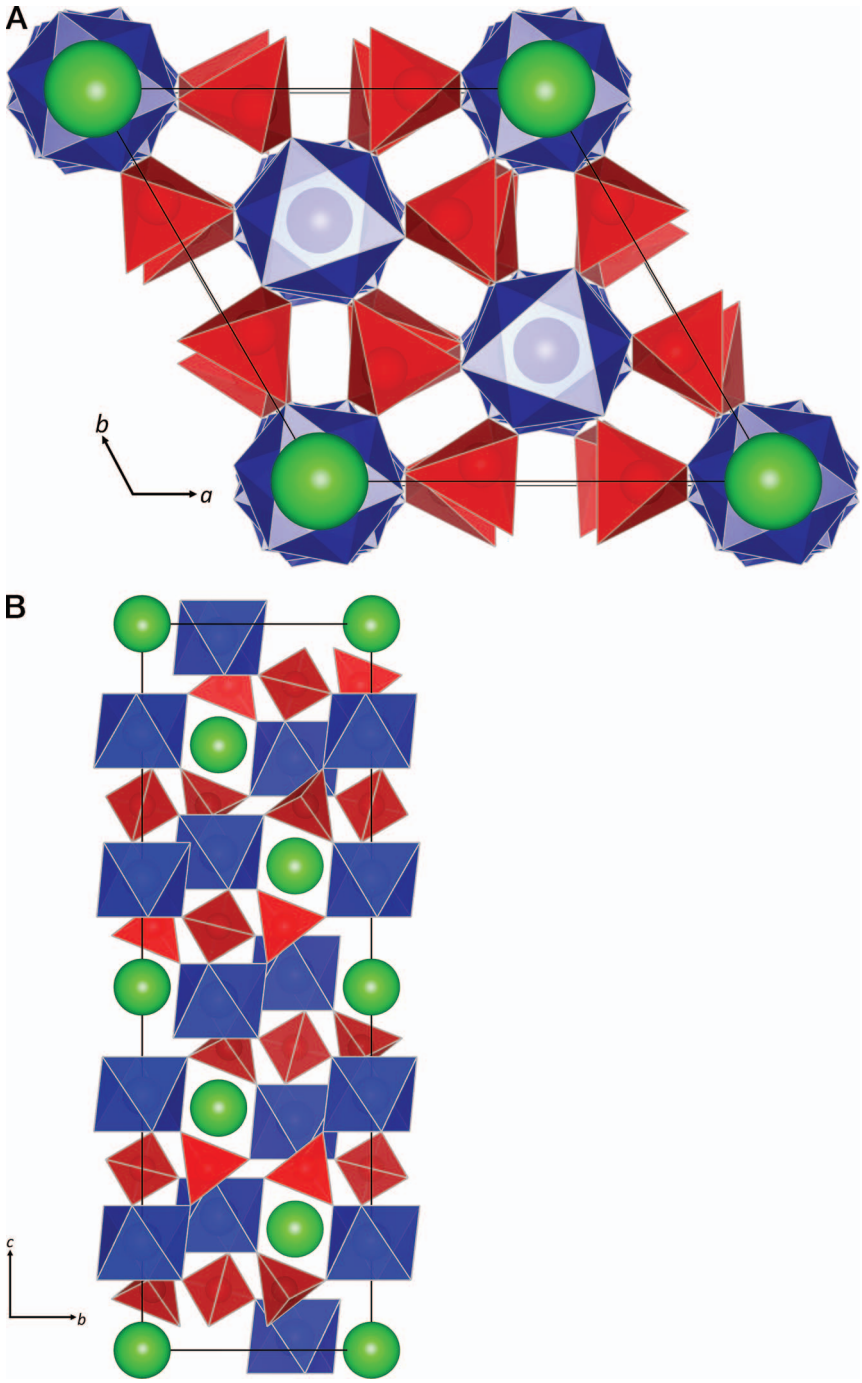

FIG. 3. (A) The crystal structure of kosnarite viewed down **c**. Red: PO_4 tetrahedra, Blue: ZrO_6 octahedra, Purple: K (M') site. (B) The local environment around the M' site in kosnarite.

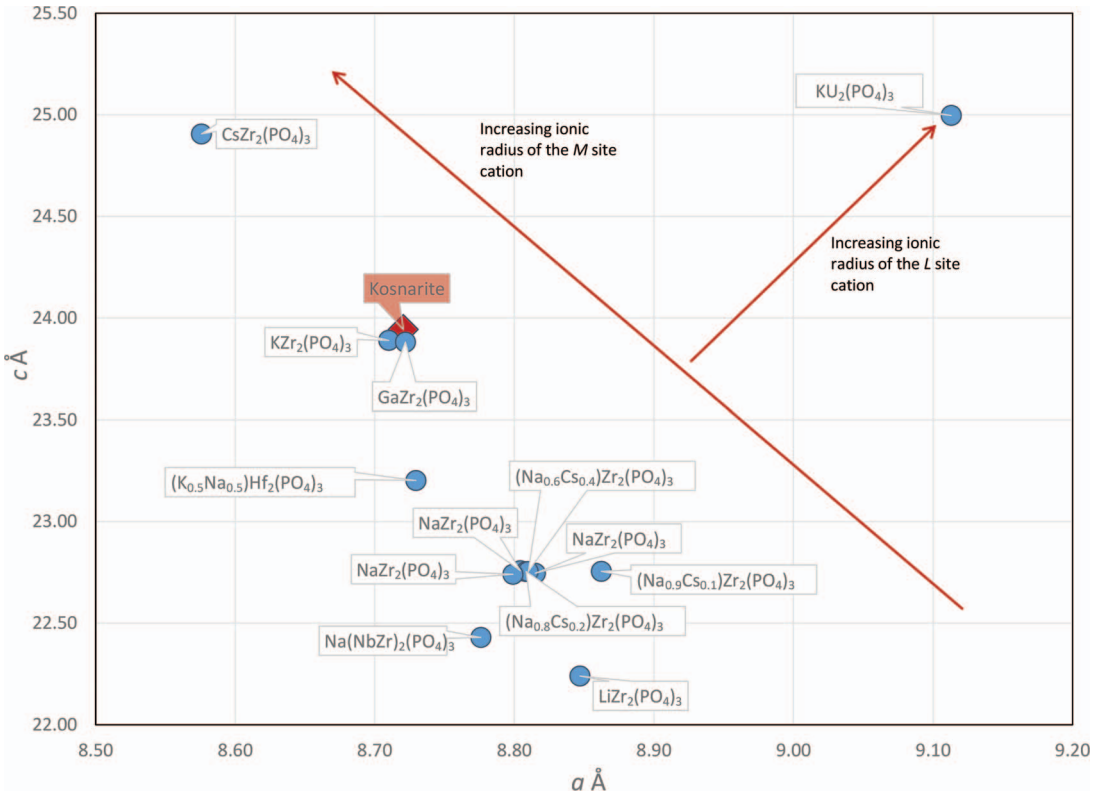

FIG. 4. Unit cell parameters, *a versus c* (Å), for kosnarite and other NZP. With increasing ionic radius of the *M*-site cation, there is a negative correlation between the lengths of the *a* and *c* axes. With increasing ionic radius of the *L*-site cation, there is a deviation from the main trend with increases in both the *a* and *c* parameters.

In theory, and as has been observed in the synthetic equivalents, with the exception of those grown in aqueous solutions, a solid solution exists between $KZr_2(PO_4)_3$ and $NaZr_2(PO_4)_3$, as well as between $KZr_2(PO_4)_3$ and $KHf_2(PO_4)_3$ (Asabina *et al.* 2010, Martynov *et al.* 2015). Compared with synthetic NZP, kosnarite has cell parameters almost identical to that of $KZr_2(PO_4)_3$. It has been shown that the Hf ↔ Zr substitution, the only other major compositional difference in natural kosnarite from all localities, has no influence on the structure of NZP (Scheetz *et al.* 1994, Deditius *et al.* 2015), therefore the minor deviation is likely the result of minor amounts of Si substituting for P. Extensive substitution of Si for P, or elements such as Th, U, or Ti for Zr, coupled with necessary charge-balancing Na at the *M″* site, also results in a destabilization of the NZP structure and reduction to monoclinic symmetry (Asabina *et al.* 2010, Martynov *et al.* 2015).

An increase in K has the ability to minimize distortions in the MO_6 and LO_6 octahedra, and therefore lower the overall energy of the kosnarite structure. So far, a natural Na endmember of kosnarite has not been found, and only limited Na ↔ K substitutions are observed in reported kosnarite compositions. It is possible that the limited substitutions for K observed in natural kosnarite are a function of the need for a lower overall energy and decreased distortions in the MO_6 and LO_6 octahedra at the crystallization conditions. In addition, kosnarite exists only as a late-stage hydrothermal/post-magmatic mineral. Observations made by Martynov *et al.* (2015), who studied the distributions of cations between the NZP structure and aqueous solutions at 200 °C, indicate that $KZr_2(PO_4)_3$ preferentially incorporates K over Na in such conditions, resulting in almost Na-free compositions (K = 0.98 – 1.0 *apfu*); lower temperature conditions would further increase this extreme partitioning. It is possible that an Na endmember is not possible in nature at the geological conditions under which kosnarite has been found thus far. Based on the distortion data for both the MO_6 and LO_6 octahedra (Fig. 5), an ideal kosnarite endmember would be $LiZr_2(PO_4)_3$.

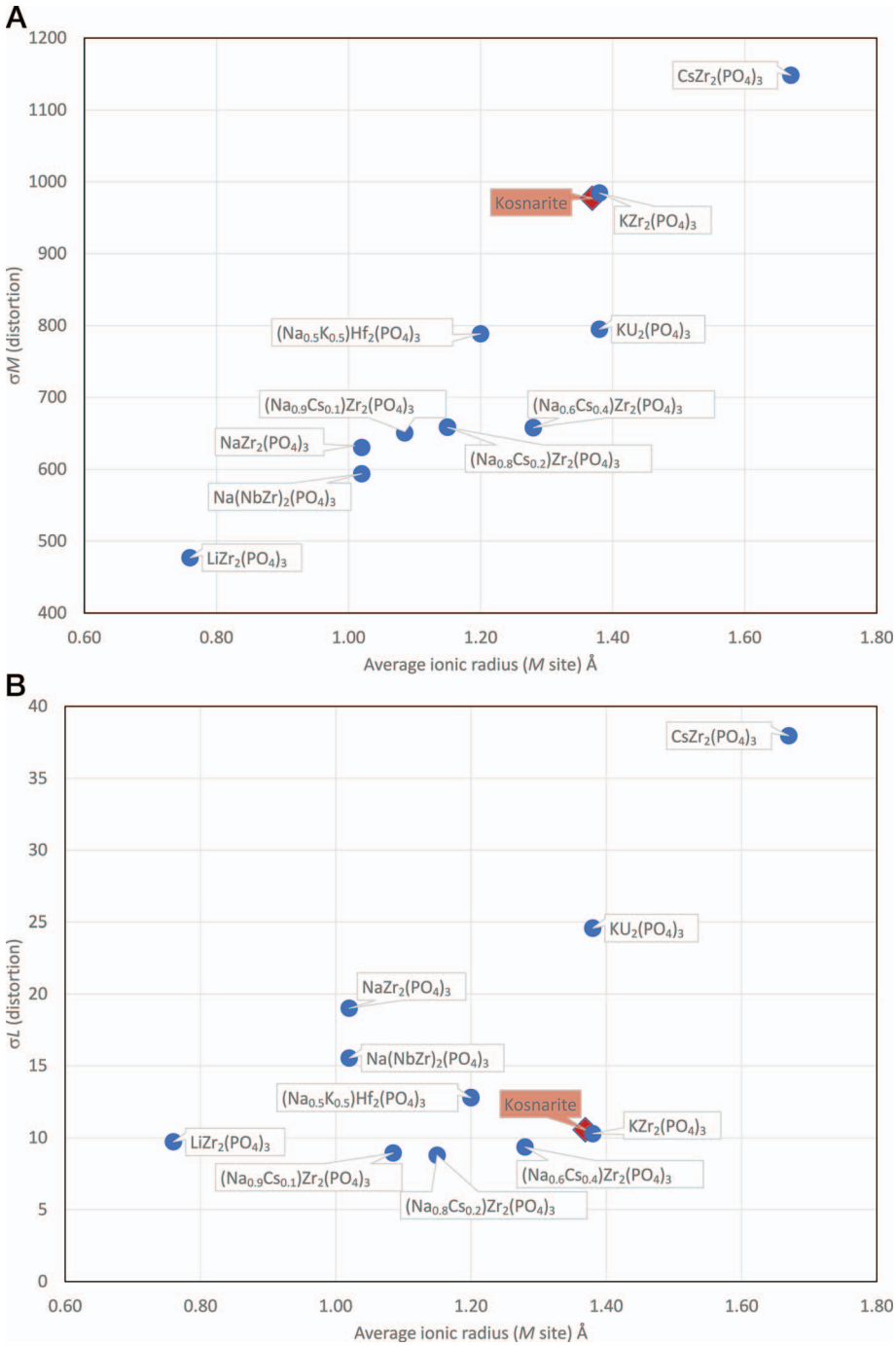

FIG. 5. (A) Average ionic radius at the *M* site versus σ*M*. (B) Average ionic radius at the *M* site versus σ*L*.

Discussion

Kosnarite is one of only five natural alkali zirconoorthophosphates: gainesite, $Na_2(Be,Li)Zr_2(PO_4)_4 \cdot 1.5H_2O$ (Moore *et al*. 1983); mccrillisite, $NaCs(Be,Li)Zr_2(PO_4)_4 \cdot 1–2H_2O$ (Foord *et al*. 1994); and selwynite, $NaKBeZr_2(PO_4)_4 \cdot 2H_2O$ (Birch *et al*. 1995), which are isostructural, along with wycheproofite, $NaAlZr(PO_4)_2(OH)_2 \cdot H_2O$. All of these are rare, secondary hydrothermal minerals that occur predominantly in granitic pegmatites at only a few localities worldwide. High-field strength elements (HFSE) such as Zr are generally considered to be insoluble in hydrothermal fluids and immobile; however, there is growing evidence that the melt or fluid chemistry can have a profound effect on the solubility of HFSE. High mobility is most common in alkaline magmas enriched in F and alkalis (Na+K), where zirconium shows a high solubility and highly incompatible nature in the melt until the final stages of crystallization. Zirconium is thought to be mobilized *via* mixed OH-F complexes in fluids with high F activity and an absence of Ca (Salvi *et al*. 2000). With increasing polymerization, Zr begins to act as a network former, resulting in increased bonding between ZrO_6 and SiO_4 groups and formation of charge-balanced $^{[6]}Zr–O–(Si,Na)$ bonds, leading to the ultimate formation of late-stage alkali zirconosilicates.

In the majority of granitic pegmatites, zirconosilicates are not present. In those pegmatites containing kosnarite, primary Zr minerals such as zircon are absent or present as only a minor phase. Kosnarite from the Jenipapo, Brazil, pegmatites is a late-stage mineral found in miarolitic cavities associated with albite, muscovite, and quartz, along with a suite of secondary phosphates including eosphorite, fluorapatite, zanazziite, montebrasite, and ushkovite (Frost *et al*. 2012). In the Maine pegmatites, kosnarite occurs as a late-stage alteration product along with gainesite, eosphorite, fluorapatite, moraesite, and quartz in small vugs developed in siderite and massive apatite (Brownfield *et al*. 1993); zircon is only a minor phase in the early stages of pegmatite crystallization. In the Wycheproof pegmatites in Australia, the crystallization sequence of kosnarite–selwynite–wycheproofite in the pegmatite vein suggests crystallization from a late-stage, secondary hydrothermal fluid with increasing Na/K as temperature decreased (Birch *et al*. 1994, Birch *et al*. 1995); no primary zircon is found in the pegmatites. Zigrasite, $MgZr(PO_4)_2 \cdot 4H_2O$, and its Ca-analogue, also from the Oxford County, Maine pegmatites, is one of the last minerals to form in the pockets (Hawthorne *et al*. 2009); zircon is found in the main pegmatite body, yet is unaltered and there is no evidence it is the source of Zr for the kosnarite (Hawthorne *et al*. 2009).

Hydrothermal experiments (Martynov *et al*. 2015) indicate that kosnarite preferentially takes up K from the fluid, resulting in compositions close to those observed in natural kosnarite. In granitic and other hydrothermal systems, the presence of ligands such as $OH^–$ and $HPO_4^{2–}$ have been shown to increase the mobility of HFSE (Migdisov *et al*. 2011, Linnen *et al*. 2014). Deditius *et al*. (2015) examined kosnarite from the advanced argillic zone at the Chaquicocha gold deposit in Peru and calculated stability diagrams. They proposed that its presence is the result of mobilization of Hf and Zr under low temperature (100–170 °C), in highly acidic conditions (pH < 5), with a high $HPO_4^{2–}$ activity, low *a*Ca and *a*F, and dominated by Zr–OH complexes. Although $ZrF(OH)_2$ and $ZrF(OH)_3$ complexes are commonly suggested for mobilization of Zr (Salvi *et al*. 2000, Migdisov *et al*. 2011), the presence of F in a granitic or epithermal deposit with high to moderate *a*Ca would result in crystallization of fluorapatite. In granitic pegmatites, it is likely that the source of the Zr is not the result of alteration of primary zircon-bearing minerals, but the result of late-stage concentration of Zr in the final fluid stage.

Conclusions

The crystal structure of a natural kosnarite has been determined for the first time. Given the wide compositional range of synthetic analogues, it is to be expected that kosnarite analogues, in particular $NaZr_2(PO_4)_3$, would be more prevalent in the natural world. The lack of a natural Na-analogue of kosnarite is likely the result of the structure's inability to incorporate Na at the low (200 °C) temperatures and highly acidic conditions in which kosnarite forms without significant distortions in the MO_6 and LO_6 octahedra, resulting in instability. Higher *a*Na in the melt or hydrothermal fluid at these conditions results in a further partitioning of K and Na, increasing the likelihood of K-dominant kosnarite forming.

Acknowledgments

The authors thank Associate Editor Frédéric Hatert, Tony Kampf, and an anonymous reviewer for their comments and suggestions to improve this manuscript. Funding for this project was provided to P.C. Piilonen in the form of a RAC grant from the Canadian Museum of Nature.

References

Alamo, J. & Roy, R. (1986) Crystal chemistry of the $NaZr_2(PO_4)_3$, NZP or CTP, structure family. *Journal of Materials Science* **21**, 444–450.

ARMSTRONG, J.T. (1988) Quantitative analysis of silicate and oxide minerals: Comparison of Monte Carlo, ZAP and phi-rho-Z procedures. *In* Microbeam Analysis (D.E. Newbury, ed.). San Francisco Press, San Francisco, California, United States (239–246).

ASABINA, E.A., PET'KOV, V.I., RUSAKOV, D.A., LAZORYAK, B.I., & KURAZHKOVSKAYA, V.S. (2010) The study of the crystalline phosphates of kosnarite type structure containing different alkali metals. *Journal of Solid State Chemistry* **183**, 1980–1984.

BENNOUNA, L., ARSALANE, S., BROCHU, R., LEE, M., CHASSAING, J., & QUARTON, M. (1995) Spécificités des ions Nb^{IV} et Mo^{IV} dans les monophosphates de type Nasicon. *Journal of Solid State Chemistry* **114**, 224–229.

BIRCH, W.D., PRING, A., & BEVAN, D. (1994) Wycheproofite: A new hydrated sodium aluminium zirconium phosphate from Wycheproof, Victoria, Australia, and a new occurrence of kosnarite. *Mineralogical Magazine* **58**, 635–639.

BIRCH, W.D., PRING, A., & FOORD, E.E. (1995) Selwynite, $NaK(Be,Al)Zr_2(PO_4)_4{\cdot}2H_2O$, a new gainesite-like mineral from Wycheproof, Victoria, Australia. *Canadian Mineralogist* **33**, 55–58.

BROWN, I.D. & SHANNON, R.D. (1973) Empirical bond-strength-bond-length curves for oxides. *Acta Crystallographica Section A* **29**, 266–282.

BROWNFIELD, M.E., FOORD, E.E., SUTLEY, S.J., & BOTINELLY, T. (1993) Kosnarite, $KZr_2(PO_4)_3$, a new mineral from Mount Mica and Black Mountain, Oxford County, Maine. *American Mineralogist* **78**, 653–656.

CHOURASIA, R., BOHRE, A., AMBASTHA, R.D., SHRIVASTAVA, O. & WATTAL, P. (2010) Crystallographic evaluation of sodium zirconium phosphate as a host structure for immobilization of cesium. *Journal of Materials Science* **45**, 533–545.

CROMER, D.T. & MANN, J.B. (1968) X-ray scattering factors computed from numerical Hartree-Fock wave functions. *Acta Crystallographica*, 321–324.

CROMER, D.T. & LIBERMAN, D. (1970) Relativistic calculation of anomalous scattering factors for X-rays. *Journal of Chemical Physics* **53**, 1891–1898.

DEDITIUS, A.P., UTSUNOMIYA, S., SANCHEZ-ALFARO, P., REICH, M., EWING, R.C., & KESLER, S.E. (2015) Constraints on Hf and Zr mobility in high-sulfidation epithermal systems: Formation of kosnarite, $KZr_2(PO_4)_3$, in the Chaquicocha gold deposit, Yanacocha district, Peru. *Mineralium Deposita* **50**, 429–436.

FOORD, E.E., BROWNFIELD, M.E., LICHTE, F.E., DAVIS, A.M., & SUTLEY, S.J. (1994) Mccrillisite, $NaCs(Be,Li)Zr_2(PO_4)_4{\cdot}1–2H_2O$, a new mineral species from Mount Mica, Oxford County, Maine, and new data for gainesite. *Canadian Mineralogist* **32**, 839–842.

FROST, R.L., XI, Y., SCHOLZ, R., & BELOTTI, F.M. (2012) Infrared and Raman spectroscopic characterization of the phosphate mineral kosnarite $KZr_2(PO_4)_3$ in comparison with other pegmatitic phosphates. *Transition Metal Chemistry* **37**, 777–782.

GOBECHIYA, E., KABALOV, Y.K., PET'KOV, V., & SUKHANOV, M. (2004) Crystal structures of double cesium zirconium and barium zirconium orthophosphates. *Crystallography Reports* **49**, 741–746.

GOBECHIYA, E., KABALOV, Y.K., TOMILIN, S., LUKINYKH, A., LIZIN, A., & ORLOVA, A. (2005) Refinement of the crystal structure of rhombohedral $KU_2(PO_4)_3$ as a representative of orthophosphates with the $NaZr_2(PO_4)_3$ structure. *Crystallography Reports* **50**, 374–378.

HAGMAN, L.-O. & KIERKEGAARD, P. (1968) The crystal structure of $NaMe_2^{IV}(PO_4)_3$; Me^{IV}= Ge, Ti, Zr. *Acta Chemica Scandinavica* **22**, 1822–1832.

HAWTHORNE, F., BALL, N., SIMMONS, J., & SIMMONS, W. (2009) Zigrasite, $MgZr(PO_4)_2(H_2O)_4$, a new phosphate mineral from the Dunton Quarry, Newry, Oxford County, Maine, USA. *Mineralogical Magazine* **73**, 415–420.

HYRSL, J., CHUKANOV, N., & SEJKORA, J. (2003) Die weltbesten Kosnarite aus Brasilien und das Amblygonit-Montebrasit-Problem. *Mineralien-Welt* **14**, 60–63.

LINNEN, R.L., SAMSON, I.M., WILLIAMS-JONES, A.E., & CHAKMOURADIAN, A. (2014) Geochemistry of the rare-earth element, Nb, Ta, Hr and Zr deposits. 2nd Edition, *Treatise on Geochemistry* **13**, 543–568.

MARTYNOV, K., AKHMEDZHANOVA, G., KOTEL'NIKOV, A., TANANAEV, I., & MYASOEDOV, B. (2015) Synthesis and study of structural analogs of kosnarite mineral under hydrothermal conditions. *Radiochemistry* **57**, 356–365

MCARDLE, P. (2017) Oscail, a program package for small-molecule single-crystal crystallography with crystal morphology prediction and molecular modelling. *Journal of Applied Crystallography* **50**, 320–326.

MENEZES FILHO, L.A.D., DE SÁ CARNEIRO CHAVES, M.L., DIAS, C., & ATENCIO, D. (2016) Recent mineral discoveries in the Coronel Murta, Taquaral, and Medina pegmatite fields, northeastern Minas Gerais, Brazil. *International Engineering Journal* **69**, 301–307.

MIGDISOV, A.A., WILLIAMS-JONES, A.E., VAN HINSBERG, V., & SALVI, S. (2011) An experimental study of the solubility of baddeleyite (ZrO_2) in fluoride-bearing solutions at elevated temperatures. *Geochemica et Cosmochimica Acta* **76**, 7426–7434.

MOORE, P.B., ARAKI, T., STEELE, I.M., SWIHART, G.H., & KAMPF, A.R. (1983) Gainesite, sodium zirconium, beryllophosphate; a new mineral and its crystal structure. *American Mineralogist* **68**, 1022–1028.

ORLOVA, A. (2002) Isomorphism in crystalline phosphates of the $NaZr_2(PO_4)_3$ structural type and radiochemical problems. *Radiochemistry* **44**, 423–445.

ORLOVA, A., CHARLAMOVA, A., & VOLKOV, Y.F. (2002) Investigation of plutonium, americium and curium phosphates as a basis for inclusion into kosnarite-type ceramic waste forms. Review of Excess Weapons Plutonium Disposition, LLNL Contract Work in Russia, 407–418.

PETIT, D., COLOMBAN, P., COLLIN, G., & BOILOT, J. (1986) Fast ion transport in $LiZr_2(PO_4)_3$: Structure and conductivity. *Materials Research Bulletin* **21**, 365–371.

ROBINSON, K., GIBBS, G., & RIBBE, P. (1971) Quadratic elongation: A quantitative measure of distortion in coordination polyhedra. *Science* **172**, 567–570.

ROWE, R. (2009) New statistical callibration approach for Bruker AXS D8 Discover microdiffractometer with Hi-Star detector using GADDS software. *Powder Diffraction* **24**, 263–271.

ROY, R., YANG, L.J., ALAMO, J., & PFOERTSCH, D.E. (1983) A single phase [NZP] ceramic radioactive waste form. *Scientific Basis for Nuclear Waste Management* **6**.

SALVI, S., FONTAN, F.O., MONCHOUX, P., WILLIAMS-JONES, A.E., & MOINE, B. (2000) Hydrothermal mobilization of high field strength eelements in alkaline igneous systems: Evidence from the Tamazeght Complex (Morocco). *Economic Geology* **95**, 559–576.

SCHEETZ, B., AGRAWAL, D.K., BREVAL, E., & ROY, R. (1994) Sodium zirconium phosphate (NZP) as a host structure for nuclear waste immobilization: A review. *Waste Management* **14**, 489–505.

SHANNON, R.D. (1976) Revised effective ionic radii and systematic studies of interatomic distances in halides and chalcogenides. *Acta Crystallographica Section A* **32**, 751–767.

SHELDRICK, G.M. (1997) *SHELXS-97 and SHELXL-97, Program for crystal structure solution and refinement*. University of Gottingen, Gottingen, Germany.

ŠLJUKIĆ, M., MATKOVIĆ, B., PRODIĆ, B., & ANDERSON, D. (1969) The crystal structure of $KZr_2(PO_4)_3$. *Zeitschrift für Kristallographie-Crystalline Materials* **130**, 148–161.

Received May 4, 2020. Revised manuscript accepted July 1, 2020.